
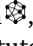





# Sodium salts of 6-hydroxy-azolo[1,5-a]pyrimidine-5-carbonitriles as red-emissive fluorescent chemosensors for picric acid

Semen V. Aminov <sup>a</sup>, Victor V. Fedotov <sup>a\*</sup> , Dmitry S. Kopchuk <sup>ab</sup>,  
Ekaterina A. Kudryashova <sup>ab</sup>, Yulia M. Sayfutdinova <sup>a</sup>, Timofey D. Moseev <sup>a</sup>,  
Mikhail V. Varaksin <sup>ab</sup>, Anton N. Tsmokalyuk <sup>a</sup>, Grigoriy V. Zyryanov <sup>ab</sup>,  
Vladimir L. Rusinov <sup>ab</sup>

**a:** Department of Organic and Biomolecular Chemistry, Ural Federal University named after the First President of Russia B. N. Yeltsin , Ekaterinburg, 620062, Russia

**b:** Postovsky Institute of Organic Synthesis , Ural Branch of the Russian Academy of Sciences, Ekaterinburg, 620066, Russia

\* Corresponding author: [viktor.fedotov@urfu.ru](mailto:viktor.fedotov@urfu.ru)

## Abstract

This paper deals with the synthesis and a comprehensive study of the photophysical and sensing properties of sodium salts of 6-hydroxy-azolo[1,5-a]pyrimidine-5-carbonitriles. The target compounds were obtained in good to high yields (81–95%) via the reaction of the corresponding 6-hydroxy-azolopyrimidines with sodium hydroxide in an aqueous ethanol. Study of the optical characteristics revealed that the synthesized compounds could be considered as red fluorophores exhibiting an intense fluorescence with emission maxima in the range of 567–597 nm with up to 55% PLQYs. The sensing properties of the obtained fluorophores were examined towards a series of nitroaromatic compounds (NACs), namely picric acid (PA), 2,4-dinitrotoluene, and 2,4,6-trinitrotoluene. The compounds exhibited a pronounced and selective fluorescence response to PA in DMSO solution, whereas no sensory effect was observed in the presence of 2,4-dinitrotoluene or 2,4,6-trinitrotoluene. As a result, a well-pronounced and selective fluorescence “turn-off” response towards PA in DMSO solution was observed with Stern-Volmer constant values of up to  $5.77 \times 10^6 \text{ M}^{-1}$ , whereas no sensory effect was observed for 2,4-dinitrotoluene (DNT) or 2,4,6-trinitrotoluene (TNT). Furthermore, the reversibility of the fluorescence response to acidic analytes was demonstrated using trifluoroacetic acid as a model compound.

## Key findings

- New azolo[1,5-a]pyrimidines sodium salts were synthesized in high yields (81–95%)
- These azolo[1,5-a]pyrimidines exhibited an intensive red-emission with photoluminescence quantum yields (PLQYs) of up to 55%
- A highly selective and sensitive fluorescence “turn-off” fluorescence response towards picric acid (PA) was observed with Stern-Volmer constants values of up to  $K_{sv} = 5.77 \times 10^6 \text{ M}^{-1}$

© 2026, the Authors. This article is published in open access under the terms and conditions of the Creative Commons Attribution (CC BY) license (<http://creativecommons.org/licenses/by/4.0/>), which permits unrestricted reuse of the work in any medium provided the original work is properly cited.

## Accompanying information

### Article history

Received: 15.01.2026

Revised: 12.02.2026

Accepted: 19.02.2026

Available online: 19.02.2026

### Keywords


Azolo[1,5-a]pyrimidines  
fluorophores  
Fluorescent chemosensors  
Nitroaromatics  
Picric acid detection

### Funding

The study was supported by the grant of the Russian Science Foundation No. 24-73-00144, <https://rscf.ru/project/24-73-00144/>.

### Supplementary information

Supplementary materials: 

Transparent peer review: 

### Sustainable Development Goals



## 1. Introduction

Against the backdrop of rapid developments in materials science, organic fluorescent molecular systems continue to

attract considerable attention from researchers due to their combination of structural diversity, high chemical stability, and broad possibilities for fine-tuning their photophysical properties. These features account for the growing demand

for organic luminescent systems in sensorics [1], biovisualization [2–4], and the development of functional optoelectronic devices [5–7]. One of the key research directions in this field is the design of conjugated organic molecules containing covalently linked donor (D) and acceptor (A) moieties. It is well established that variations in the electronic nature of the donor and acceptor units, as well as changes in the length and nature of the  $\pi$ -conjugated bridges between them, have a significant influence on the optical properties of D–A and related systems.

In this context, azolo[1,5-a]pyrimidines represent promising electron-acceptor molecules. Although this class of heterocycles has traditionally been studied in medicinal chemistry [8,9], their electronic structure makes these compounds attractive for use in donor–acceptor fluorescent systems. The possibility of structural modification of the azolo[1,5-a]pyrimidine core enables fine-tuning of its electron-withdrawing properties, which significantly expands the design potential of functional organic photoactive molecular systems.

The importance of fluorescent molecules based on azolo[1,5-a]pyrimidines and their practical applicability have been demonstrated by numerous studies conducted by various research groups. In recent years, azolopyrimidine-based luminophores have attracted particular attention due to their high luminescence quantum yields in both solution and the solid state, as well as their photostability [10]. These properties have led to the widespread applications of azolo[1,5-a]pyrimidine fluorophores as sensitizers in solar cells [11], components of hybrid dyes [12], and biomarkers [13]. Furthermore, the unique electronic characteristics of these compounds make them promising candidates for the development of fluorescent chemosensors capable of selectively detecting various analytes, including nitroaromatic compounds (NACs) [14].

Nitroaromatic compounds (NACs) are an important class of organic compounds whose molecules contain one or more nitro groups ( $-\text{NO}_2$ ) attached to an aromatic ring. These compounds represent one of the most widely used classes of organic substances and have found applications in various fields of human activity. NACs are extensively used in the chemical, dye, and pharmaceutical industries [15]. In addition, compounds such as 2,4,6-trinitrotoluene (TNT), 2,4-dinitrotoluene (DNT), and 1,3,5-trinitrobenzene (TNB) still widely employed in explosives blends or as propellants.

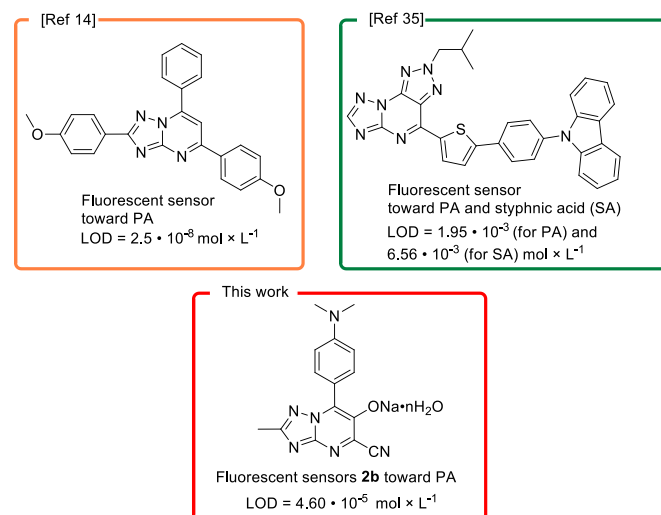
Due to their high detonation potential and relative safety in handling, NACs are widely used in the military industry, the mining sector, and pyrotechnics [16–18]. However, the ease of synthesis, availability of raw materials, and stability of NACs also make them attractive for the manufacture of improvised explosive devices. This poses a serious threat to public safety in crowded areas such as airports, train stations, concert venues, and other infrastructure facilities. Furthermore, NACs are highly toxic and carcinogenic and can accumulate in the environment, posing a

significant threat to ecosystems [19]. This problem is particularly acute in combat zones, minefields, and explosive disposal sites.

A wide range of analytical methods have currently been used to detect NACs, including gas chromatography–mass spectrometry (GC–MS) [20], surface-enhanced Raman spectroscopy (SERS) [21,22], electrochemical detection [21], and enzyme-linked immunosorbent assay (ELISA) [23]. Despite their high accuracy, these methods have several significant drawbacks: they require expensive equipment and highly qualified personnel, involve long analysis times, are limited in mobility, and are prone to false-positive or false-negative results [24,25]. In this regard, fluorescence-based detection represents a promising alternative, as it is characterized by high sensitivity, convenience, and ease of use [26,27]. This method is based on changes in emission characteristics (e.g., emission band shifts, signal enhancement, or quenching) that occur upon interaction of a fluorophore with an analyte, enabling the detection of NACs, including by visual observation, without the need for complex equipment.

Among NACs, 2,4,6-trinitrophenol (also known as TNP or picric acid (PA)) has found the widest practical application due to its higher explosive power compared with other compounds of this class [28,29]. A distinctive feature of TNP is its ability to dissociate in aqueous media to form an anion, along with pronounced acidic properties ( $\text{pK}_a = 0.38$ ), which distinguishes it from neutral molecules such as TNT, TNB, DNB, and related compounds. Owing to these characteristics, TNP can be effectively detected using acid–base and ion-exchange reactions.

Currently, numerous chemosensors have been developed for the detection of NACs, including metal–organic frameworks (MOFs) [30], nanomaterials [31], and organic heterocyclic compounds [32–34]. Despite the relatively limited number of reported examples, existing studies demonstrate the high selectivity of azolo[1,5-a]pyrimidines for the detection of TNP and other NACs [14,35] in organic solutions (Figure 1).



**Figure 1** Fluorescent chemosensors based on azolo[1,5-a]pyrimidine scaffold

We previously developed an efficient synthetic approach to 6-hydroxy-azolo[1,5-a]pyrimidine-5-carbonitriles and demonstrated the feasibility of obtaining their stable salt forms [36]. In the present study, we carried out the targeted synthesis of the corresponding sodium salts, followed by a comprehensive study of their photophysical properties and sensing behavior. Particular attention was devoted to the analysis of the selectivity of the interactions between the obtained compounds and PA, which confirmed their potential as chemosensors for the selective detection of PA.

## 2. Results and discussion

### 2.1. Synthesis of chemosensors

We previously reported a synthesis of a series of 6-hydroxy-azolo[1,5-a]pyrimidines [36], which readily formed stable salts with various bases. Based on this finding, in a frame of this work a series of sodium salts of 6-hydroxy-azolo[1,5-a]pyrimidine-5-carbonitriles was prepared. Thus, the reaction of the starting azolopyrimidines **1a-h** with sodium hydroxide in an aqueous-ethanolic medium under heating conditions led to the formation of compounds **2a-h** in high yields (81-95%), with structures being confirmed by  $^1\text{H}$  and  $^{13}\text{C}$  NMR spectroscopy. While elemental analysis and thermogravimetric measurements revealed that the resulting compounds were crystalline hydrates with varying water content (Scheme 1).

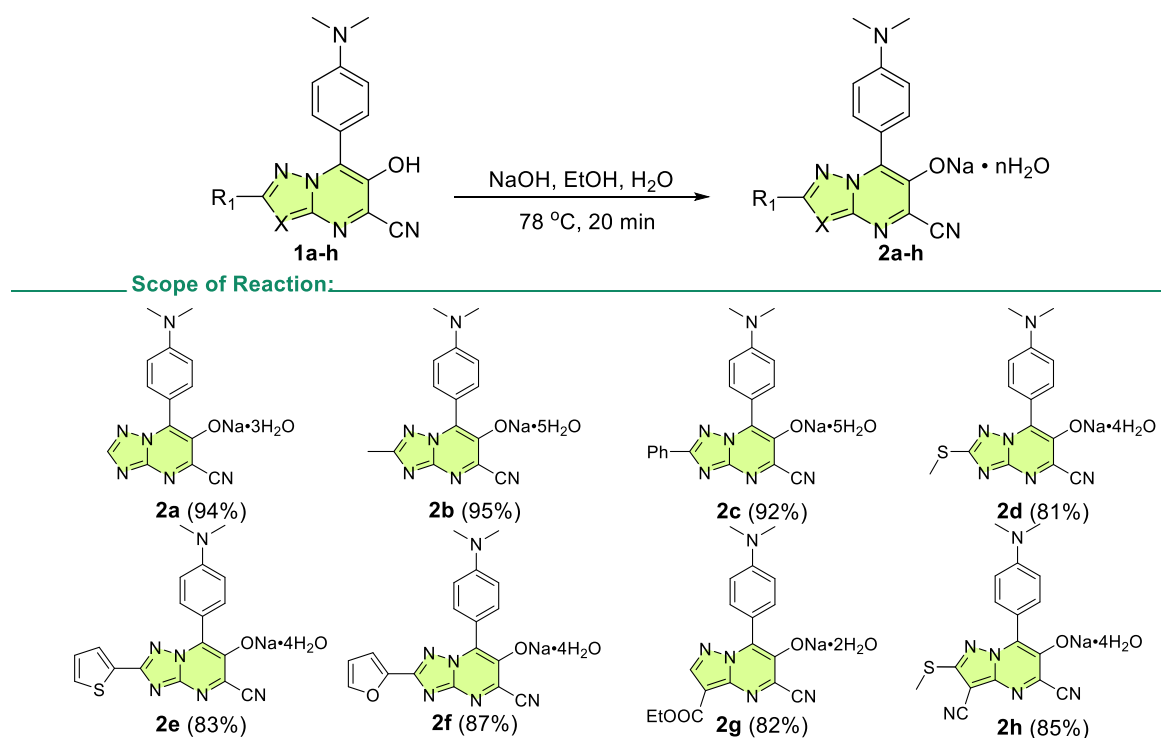
### 2.2. Photophysical properties of heterocycles **2a-h**

Photophysical properties of compounds **2a-h** were investigated in DMSO at room temperature. The resulting UV-visible and emission spectra are presented in Figure 2, and

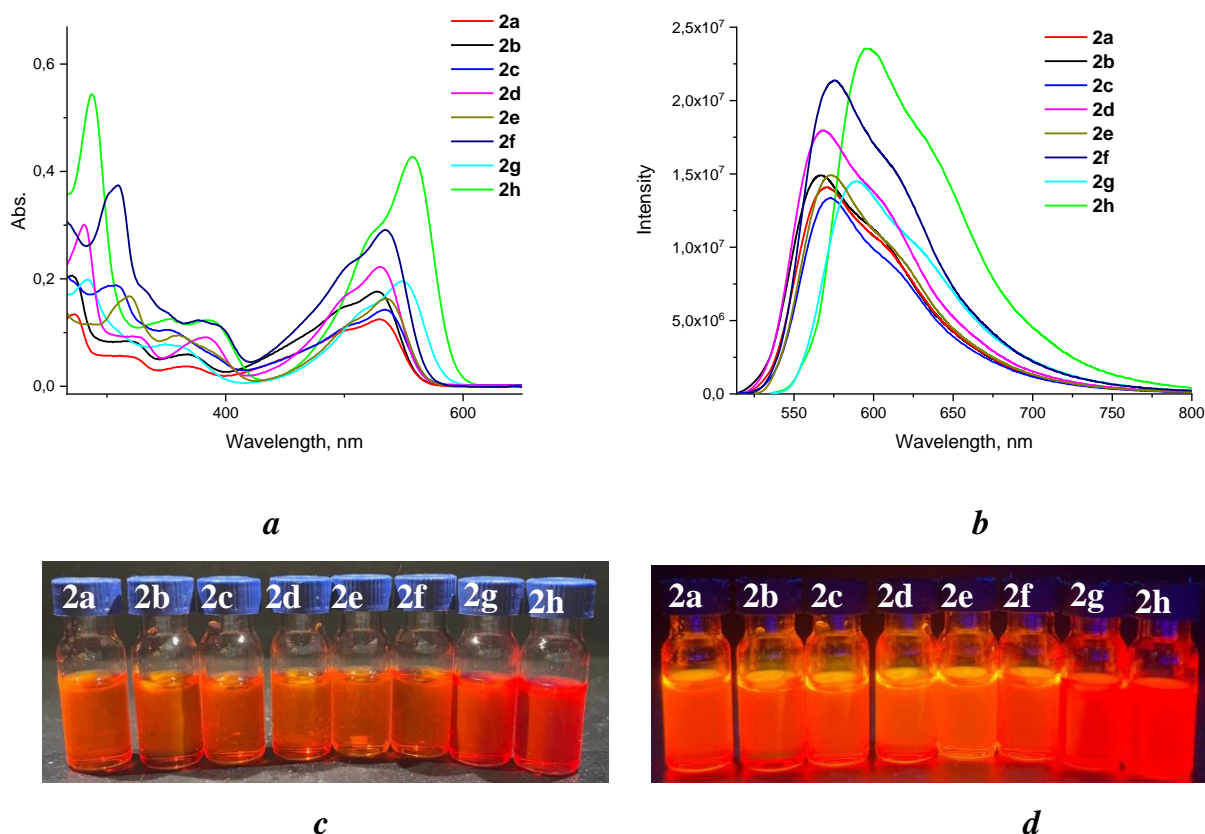
the corresponding photophysical data are summarized in Table 1.

One can observe that the UV-visible spectra, compounds **2a-h** exhibit a complex pattern with multiple absorption peaks, two of which are located at long wavelengths (527-558 nm) and in the UV-B region (290-310 nm), along with several peaks at the edge of the visible region (360-400 nm). Molar extinction coefficients reach up to  $42,700 \text{ M}^{-1} \text{ cm}^{-1}$ , suggesting that these absorption bands can be attributed to  $\pi \rightarrow \pi^*$  transitions. The fluorescence emission spectra display an intense, broadened emission band in the range of 569-597 nm range, which may be associated with either a locally excited (LE) state or an intramolecular charge transfer (ICT) state. Furthermore, quantum yields of up to 55% were recorded, highlighting their potential as red-emitting photoactive systems (Table 1).

Analysis of the photophysical properties of the **2a-h** series reveals that the nature of the azole fragment in the heterocyclic system has the most significant influence on the position of the long-wavelength absorption maxima. Namely, pyrazole-containing derivatives **2g** and **2h** were found to exhibit a bathochromic shift of 22-31 nm in their absorption maxima relative to the corresponding triazole-containing analogs, most likely due to the enhanced electron-acceptor properties of the ethoxycarbonyl and nitrile groups. In case of triazole derivatives displayed similar spectral characteristics, with their absorption maxima localized within a narrow range of approximately 530 nm. Variation of the substituents at position C2 of the heterocyclic ring was shown to have no significant effect on the absorption peak position, suggesting the dominant role of the azole fragment in the electronic transitions of this spectral region.



**Scheme 1** Synthesis of chemosensors **2a-h**.



**Figure 2** (a) Combined absorption spectra of compounds **2a-h** ( $C = 10^{-5}$  M) in DMSO at rt. (b) Combined emission spectra of compounds **2a-h** ( $V = 10^{-5}$  M) in DMSO at rt. Photographs of solutions of **2a-h** in DMSO under daylight (c) and under irradiation (d) with a hand-held UV lamp at 365 nm.

**Table 1** Photophysical properties of compounds **2a-h** in DMSO solution at rt.

N <sup>o</sup>	$\lambda_{\text{abs}}$ , nm	$\epsilon$ ( $\lambda_{\text{abs max}}$ , $\text{M}^{-1}\text{cm}^{-1}$ )	$\lambda_{\text{em}}^{\text{a}}$ , nm	$\Delta\lambda^{\text{b}}$ , nm ( $\text{cm}^{-1}$ )	$\Phi_{\text{F}}^{\text{c}}$ , %
<b>2a</b>	272, 367, 530	12500	571	41 (1355)	55
<b>2b</b>	318, 368, 527	17600	567	40 (1339)	52
<b>2c</b>	257, 308, 351, 534	14300	573	39 (1275)	55
<b>2d</b>	281, 382, 530	22200	569	39 (1293)	47
<b>2e</b>	319, 360, 535	16300	573	38 (1240)	46
<b>2f</b>	310, 377, 534	29100	576	42 (1365)	45
<b>2g</b>	283, 349, 549	19600	589	40 (1237)	39
<b>2h</b>	287, 352, 385, 558	42700	597	39 (1171)	47

<sup>a</sup> Excitation at the long-wavelength absorption maximum;

<sup>b</sup> Stokes shift was calculated relative to the lowest-energy absorption peak;

<sup>c</sup> Absolute fluorescence quantum yield was measured using a Horiba-Fluoromax-4 spectrofluorimeter equipped with an integrating sphere.

**Table 2** The lifetime of compounds **2a-h** ( $C = 2 \times 10^{-6}$  M) in DMSO solution.

N <sup>o</sup>	$\tau$ , ns <sup>a</sup>	$\alpha^{\text{b}}$	$\chi^2$ <sup>c</sup>
<b>2a</b>	6.93	1	1.09
<b>2b</b>	7.03	1	1.19
<b>2c</b>	7.10	1	1.10
<b>2d</b>	6.94	1	1.09
<b>2e</b>	7.08	1	1.19
<b>2f</b>	7.07	1	1.19
<b>2g</b>	7.37	1	1.11
<b>2h</b>	7.45	1	1.14

<sup>a</sup> Decay time;

<sup>b</sup> Partial contribution;

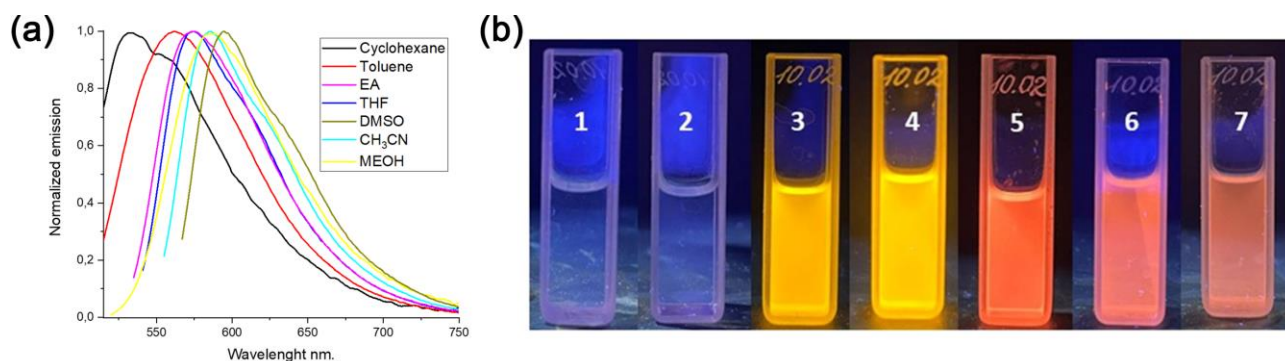
<sup>c</sup> quality of the data fit.

The average fluorescence lifetimes ( $\tau_{\text{av}}$ ) of compounds **2a-h** were also determined (Table 2). The highest  $\tau_{\text{av}}$  values were observed for the pyrazole-containing derivatives **2g** and **2h**, amounting to 7.45 and 7.37 ns, respectively. In general, relatively long lifetimes were recorded for the studied

series of azolopyrimidines, indicating increased stability of their excited states. These data suggest the formation of relatively stable singlet excited states in these heterocyclic systems, capable of sustained radiative emission, which is consistent with the high quantum yields previously reported for several derivatives.

### 2.3. Solvatochromic properties of compounds **2a-h**

Compounds **2a-h** are push-pull systems, combining an electron-withdrawing azolopyrimidine core with an electron-donating arylamino moiety, which underlies their potential to exhibit fluorescent solvatochromism. To prove that the absorption and emission spectra of the **2a-h** series were recorded in solvents of varying polarity, such as cyclohexane, toluene, tetrahydrofuran, dichloromethane, and ethyl acetate.



**Figure 3** (a) Normalized emission spectrum of compound **2h** in different solvents ( $C = 10^{-5}M$ ). Photographs of the solutions compound **2h** (b) in different solvents (1 - Cyclohexane, 2 - Toluene, 3 - THF, 4 - EtOAc, 5 -  $CH_3CN$ , 6 - DMSO, 7 - MeOH) under irradiation with a hand-held UV lamp at an emission wavelength of 380 nm.

**Table 3** Summary data from Lippert-Mataga graphs for compounds **2a-h**.

Nº	Slopes <sup>a</sup>	R <sup>2</sup> <sup>b</sup>	$\Delta\mu$ , D <sup>c</sup>
<b>2a</b>	9806	0.92	11.17
<b>2b</b>	3741	0.93	6.90
<b>2c</b>	7818	0.93	9.97
<b>2d</b>	12420	0.91	12.57
<b>2e</b>	12477	0.92	12.59
<b>2f</b>	13006	0.91	12.86
<b>2g</b>	4232	0.92	7.33
<b>2h</b>	7245	0.90	9.60

<sup>a</sup> Slope of the trend line;

<sup>b</sup> Standard deviation from the trend line;

<sup>c</sup> Difference in the dipole moments of the ground and excited states.

Upon the increase of the polarity of the solvent in all the cases the bathochromic shift of the emission maxima was suggested to take place, which confirms a moderate positive solvatochromic effect consistent with the excited-state intramolecular charge transfer (ICT) model. The nature of the spectral response depends nonlinearly on a solvent polarity. The most pronounced bathochromic shifts of the emission maxima are observed in polar and moderate polar media. In highly polar solvents such as dimethyl sulfoxide, acetonitrile, and methanol, the positions of the emission maxima remain virtually unchanged or shift only within the experimental error (Figure 3 and see Supporting Information).

The absence of a significant fluorescence shift in highly polar solvents may be attributed to the saturation of excited-state charge stabilization, as well as to the possible enhancement of solvation-controlled non-radiative relaxation pathways that compete with radiative emission. The difference in dipole moments between the ground and excited states ( $\Delta\mu$ ) for the **2a-h** series was estimated using the Lippert-Mataga equation. For all the derivatives studied, a highly linear dependence of the Stokes shift ( $\Delta\nu_{st}$ ) on the orientational polarizability function,  $\Delta f$ , is observed; correlation coefficients ( $R^2$ ) exceed 0.90 (Table 3), confirming the applicability of the chosen model. Notably, the plots for the entire series display a single linear relationship in all the solvents considered, including cyclohexane, toluene, tetrahydrofuran ethyl acetate, DMSO, and MeOH, indicating a common nature of the electronic transition with a pronounced intramolecular charge transfer (ICT) component.

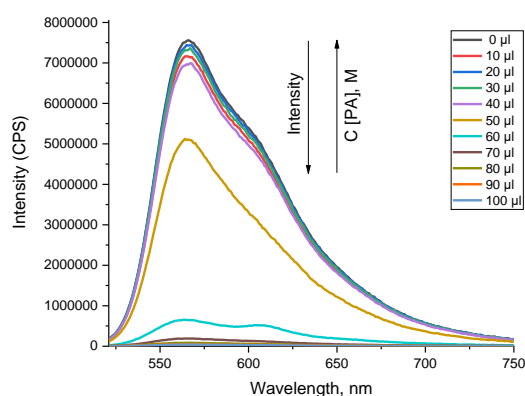
In addition, the correlation between bathochromic shift value of the emission maxima and solvent polarity was studied using Kosower scales [37] and Dimroth-Reichardt [38]. When calculating the Debye parameter, an approximation of the Onsager radius of 4 angstroms was applied [39]. The  $\Delta\mu$  values for the studied series range from 6.9 to 12.86 D (Table 3), with the maximum value of 12.86 D observed for **2f**, highlighting a significant contribution of the ICT state to the emission pattern. Molecules **2a**, **2c**, and **2e** exhibit  $\Delta\mu$  values around 12 D, suggesting a smaller, but still notable, contribution of the ICT state to radiative emission. In contrast, compounds **2b**, **2g**, and **2h** display the lowest  $\Delta\mu$  values, which may be associated with the predominance of the locally excited (LE) state during emission.

#### 2.4. Studies of sensory response of fluorophores

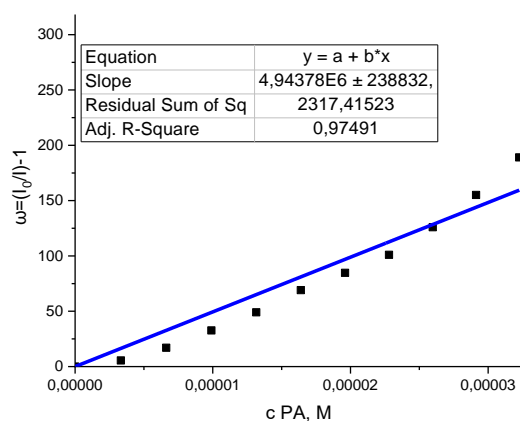
A number of NACs, including nitrobenzene, DNT, TNT, and PA, are of considerable industrial importance. These substances are used as chemical reagents, intermediates in organic synthesis, and in the production of specialty materials, including components of energetic and explosive compounds. At the same time, compounds of this class are highly toxic to living organisms, which underscores the need for methods for their selective and highly sensitive detection in both gas and liquid phases, particularly for environmental monitoring [40].

As a first step, a sensory response of fluorophores **2b** and **2g** toward PA in DMSO solutions were studied. Thus, the emission spectrum of the pure fluorophore was recorded at a concentration of  $10^{-5} M$  (in DMSO) in the absence of a quencher. Subsequently, aliquots of the analyte ( $10^{-3} M$ ) (in DMSO) were added successively to the cuvette, ensuring complete homogenization of the solution by thorough mixing before recording the fluorescence spectrum. Changes in emission intensity were recorded after each addition of PA (Figure 4).

Upon addition of 100  $\mu L$  of picric acid (PA) to fluorophore **2b**, an immediate decrease in the fluorescence quantum yield to 3% was observed. Similarly, the addition of picric acid to fluorophore **2h** resulted in an instantaneous decrease in the quantum yield: 29% at 50  $\mu L$  of PA, 17% at 100  $\mu L$ , and 11% at 200  $\mu L$ .



**Figure 4** Fluorescence quenching of fluorophore **2b** ( $10^{-5}$  M) in the presence of PA ( $10^{-3}$  M)



**Figure 5** Stern-Volmer plot of PA titration of fluorophore **2b** ( $10^{-5}$  M). The Stern-Volmer constant is  $4.94 \times 10^6$ , the standard deviation is 0.97.

Analysis of the quenching process using the Stern-Volmer equation revealed that the dependence of  $I_0/I$  on the PA concentration remained linear in the range of  $0-6 \times 10^{-5}$  M, with a correlation coefficient ( $R^2$ ) of 0.97, indicating the suitability of the selected model for describing interactions within this concentration range (Figure 5). The calculated high quenching constant,  $K_{SV} = 4.94 \times 10^6$  M $^{-1}$ , clearly indicates intensive sensory response of fluorophore **2b** towards PA.

In general, the fluorescence quenching of chemosensors by nitroaromatic analytes predominantly proceeds via a static quenching mechanism. This conclusion is supported by the linear Stern-Volmer plots as well as by the fluorescence lifetime data (Table 2). For dynamic quenching, the Stern-Volmer constant is given by  $K_{SV} = k_q \cdot \tau_0$ . Based on the experimentally determined  $K_{SV}$  values ( $6.97 \cdot 10^4 - 4.94 \cdot 10^6$  M $^{-1}$ ) and the measured fluorescence lifetimes, the calculated hypothetical bimolecular quenching rate constants  $k_q$  ( $7 \cdot 10^{14}$  M $^{-1}$  s $^{-1}$  for **2b** and  $9 \cdot 10^{12}$  M $^{-1}$  s $^{-1}$  for **2h**) would exceed the diffusion-controlled limit ( $\sim 10^{10}$  M $^{-1}$  s $^{-1}$ ) [41]. Therefore, a dynamic quenching mechanism can be excluded, and the observed quenching is attributed to a static mechanism, in agreement with literature reports on nitroaromatic sensing systems.

The detection limit (LOD) was determined based on adjusted data from fluorescence quenching experiments in accordance with the previously published method [42,43]. A

calibration curve was constructed between the fluorescence intensity and the concentration of the analyte to obtain the regression curve equation. Considering that  $\sigma$  is the standard deviation of the fluorophore intensity in the absence of the analyte, LOD was calculated using equation:

$$LOD = 3\sigma/Slope \quad (1)$$

$$LOD = 3 \cdot 1895871.26 / 1.24 \cdot 10^{11} = 4,60 \cdot 10^{-5} \text{ mol/l}$$

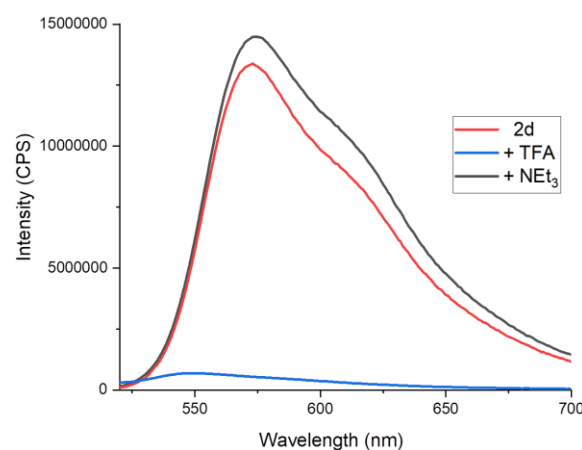
$$LOD = 10.54 \text{ ppm}$$

However, for other NACs, such as DNT and TNT, fluorophores **2b** were not found to exhibit any fluorescence response, with no significant changes in emission intensity being observed (Figure S38 and S39). The absence of quenching for these compounds highlights the pronounced selectivity of the studied fluorophore series toward PA in solutions.

The chemosensors based on sodium salts of 6-hydroxy-azolo[1,5-a]pyrimidine-5-carbonitriles developed in this work exhibit moderate sensitivity, with limits of detection in the micromolar range, in comparison with many recently reported fluorescent sensors that achieve nanomolar-level detection of picric acid [44-46]. Nevertheless, when compared with the limited number of azolopyrimidine-based chemosensors described in the literature, the obtained compounds show detection limits comparable to those previously reported [35].

Importantly, the main advantages of the developed chemosensors lie in their high fluorescence quantum yields and their potential applicability for the detection of picric acid in semi-aqueous media (DMSO/water systems).

The reversible sensing response of fluorophore **2d** to acidic analytes (using TFA as an example) was demonstrated via fluorescence quenching studies in DMSO. Addition of microliter aliquots of TFA (0.1 M) to a fluorophore solution ( $10^{-5}$  M) resulted in a significant decrease in fluorescence intensity. Subsequent addition of an equimolar amount of triethylamine fully restored the initial emission (Figure 6).



**Figure 6** Change in fluorescence of compound **2d** ( $10^{-5}$  M) upon addition of TFA (0.1 M solution, 1  $\mu$ l) and triethylamine (0.1 M solution, 1  $\mu$ l)

These results confirm the chemically reversible nature of the interaction between fluorophore **2d** and acids. A common key step in the fluorescence quenching mechanism by picric acid and TFA is the formation of a non-emissive form of the fluorophore. The reversibility of the acid–base interaction is demonstrated by the complete restoration of fluorescence upon addition of triethylamine, which regenerates the emissive form (Figure 7).

## 2.5. DFT Calculations

To rationalize the experimental absorption spectra and to elucidate the role of ionic species in determining the optical properties of the investigated compounds, quantum chemical calculations were carried out using density functional theory (DFT) and time-dependent DFT (TD-DFT). Geometry optimizations resulted in stable structures for the neutral forms of compounds **2a–f** the optimized coordinates, corresponding energetic data are provided in the Supporting Information (Table S9).

TD-DFT calculations of vertical electronic excitations for the optimized neutral molecules revealed a pronounced discrepancy with the experimental absorption spectra. In particular, the calculated spectra lack an intense absorption band associated with the experimentally observed HOMO →

LUMO transition. This inconsistency suggests that the neutral molecular forms alone cannot account for the experimentally detected optical features and indicates the involvement of alternative electronic species under the experimental conditions.

Considering the experimental setup and the polar nature of the solvent, the formation of anionic species was examined. For compound **2a**, the Gibbs free energy of solvation in DMSO was evaluated for the process leading to the formation of the corresponding anion accompanied by a  $\text{Na}^+$ -DMSO ion pair. The calculated solvation free energy ( $\Delta G_{\text{solv}} = 0.32 \text{ eV}$ ) indicates that this process is energetically favourable. This value is consistent with reported theoretical and experimental data for small and medium-sized organic molecules, thereby supporting the thermodynamic feasibility of anion formation in solution [47]. Consequently, the contribution of anionic forms must be considered when interpreting the experimental spectra.

Geometry optimizations were subsequently performed for the anionic forms of all compounds **2a–f** the corresponding data are summarized in the SI. For the anions of compounds **2b** and **2f**, excited electronic states were further investigated using TD-DFT calculations. The most probable electronic transitions associated with significant oscillator strengths are depicted in Figures 8 and 9.

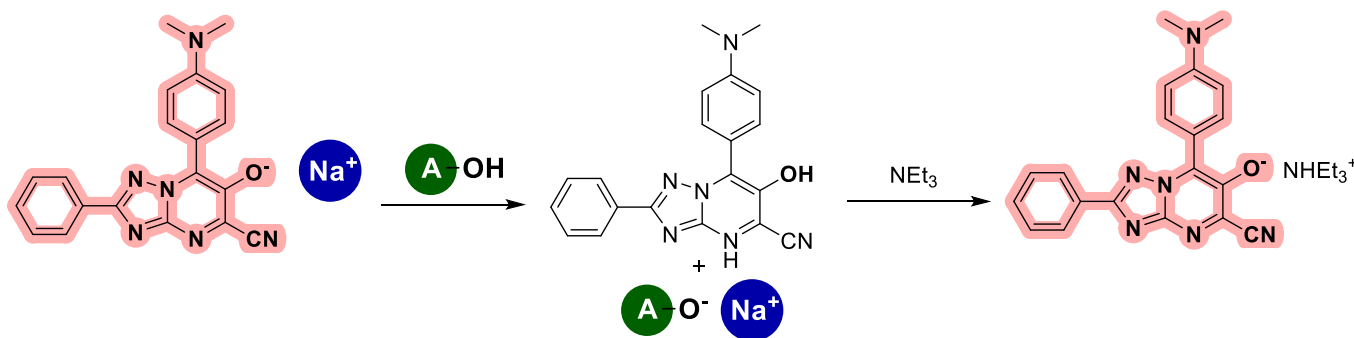


Figure 7 Mechanism of response to acidic analytes.

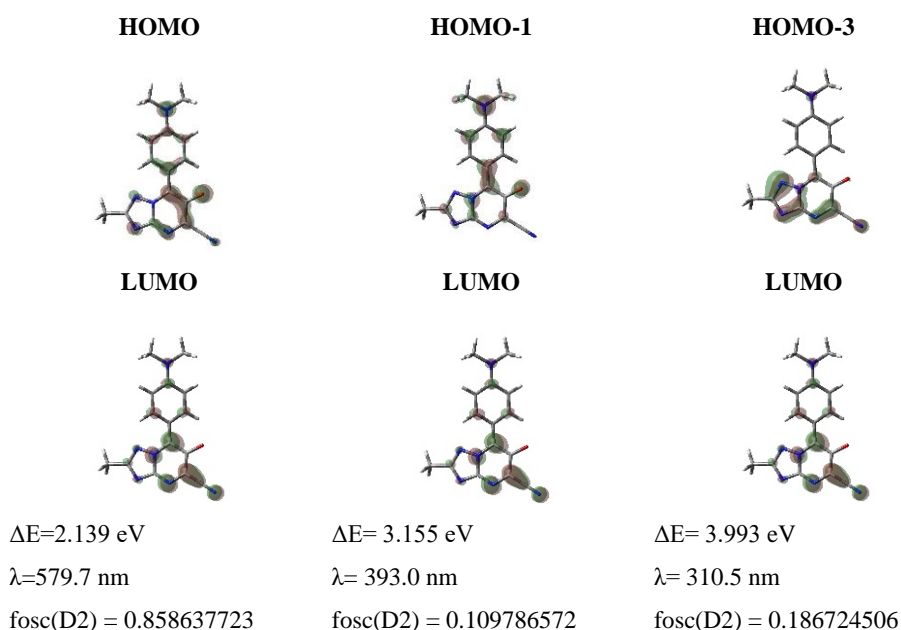
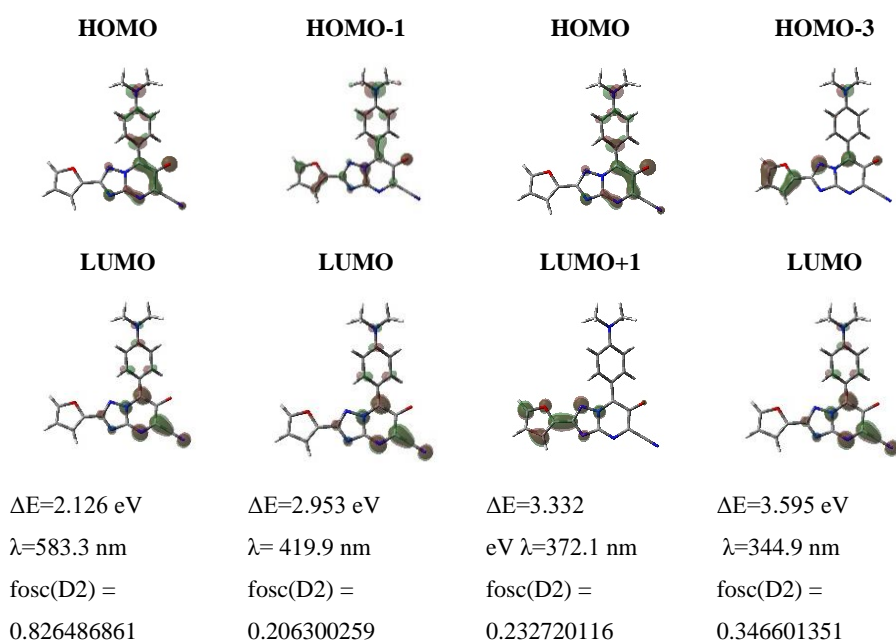


Figure 8 Probable electronic transitions in the absorption spectrum of anion **2b**.



**Figure 9** Probable electronic transitions in the absorption spectrum of anion **2f**.

For anion **2b**, the calculations successfully reproduce all three experimentally observed absorption bands. The most intense band arises from the HOMO → LUMO transition, in full agreement with experimental observations. Two additional bands originate from the HOMO<sup>-1</sup> → LUMO and HOMO<sup>-3</sup> → LUMO transitions; their markedly lower oscillator strengths indicate a reduced probability of these excitations, consistent with their weaker experimental manifestation.

In the case of anion **2f**, four absorption bands were predicted. The dominant band, exhibiting the highest oscillator strength, corresponds to the HOMO → LUMO transition. Two additional bands located in the 380–400 nm region display comparable but lower oscillator strengths and could be assigned to the HOMO<sup>-1</sup> → LUMO and HOMO → LUMO<sup>+1</sup> transitions. In the experimental spectrum, these transitions are likely manifested as a broad, unresolved absorption feature. The fourth band, with an intensity lower than that of the main transition but higher than the two intermediate ones, is associated with the HOMO<sup>-3</sup> → LUMO transition (see the Supporting Information for more details Figures S40–S48).

It should be noted that the calculated absorption maxima exhibit a systematic bathochromic shift of approximately 40 nm relative to the experimental values. This deviation can be attributed to the well-documented tendency of TD-DFT to underestimate the energies of vertical electronic excitations, as well as to the approximate treatment of solvation effects and the absence of vibronic averaging in the calculations. Such discrepancies are characteristic of this level of theory and have been extensively discussed in the literature [48].

Overall, the quantum chemical results clearly indicate that the anionic forms of compounds **2a–f** are responsible for the experimentally observed absorption features. The

calculated electronic transitions account for both the position and relative intensities of the main absorption bands, providing strong theoretical support for the proposed model in which ionic species represent the key optically active forms of these compounds in solution.

### 3. Limitations

This study has several limitations. No fluorescence response was observed for the studied compounds in the presence of other NACs, indicating the limited applicability of these azolo[1,5-*a*]pyrimidine derivatives as universal chemosensors for nitroaromatic explosives. In addition, the compounds exhibit pronounced acidochromic properties, which further restricts their practical use, as false-positive signals may arise from non-specific interactions under the experimental conditions. It should also be noted that only the sodium salts of 6-hydroxy-azolo[1,5-*a*]pyrimidine-5-carbonitriles were evaluated in this work, while the influence of the counterion on sensory properties was not considered. These limitations underscore the need for further structural optimization of 6-hydroxy-azolo[1,5-*a*]pyrimidine-5-carbonitriles derivatives to enhance selectivity and expand their potential applications as sensors.

### 4. Conclusions

In conclusion, a series of new 6-hydroxy-azolo[1,5-*a*]pyrimidine-5-carbonitriles sodium salts were synthesized, and their photophysical properties were investigated. According to the obtained results, the obtained azolo[1,5-*a*]pyrimidine derivatives can serve as fluorescent sensors for the detection of picric acid, a widely used component of explosives. The studied compounds showed no fluorescent response in the presence of other nitroaromatic analytes,

such as DNT and TNT. Furthermore, these fluorophores exhibited reversible acidochromism, which was confirmed experimentally through titration with trifluoroacetic acid. Based on the combined experimental data, it was established that fluorescence quenching upon interaction with picric acid arises from the acid–base interaction between the analyte and the sensor. Overall, the results highlight the high potential of azolopyrimidine systems for the development of new fluorescent sensors for the selective detection of picric acid.

## 5. Materials and Methods

Commercial reagents were obtained from Sigma-Aldrich, Acros Organics, Alfa Aesar or Macklin and used without any preprocessing. All workup and purification procedures were carried out using analytical-grade solvents. One-dimensional  $^1\text{H}$  and  $^{13}\text{C}$  NMR spectra were acquired on a Bruker DRX-400 instrument (Karlsruhe, Germany) (400 and 101 MHz, respectively), utilizing DMF-D7 as a solvent and an external reference, respectively. Chemical shifts are expressed in  $\delta$  (parts per million, ppm) values, and coupling constants are expressed in hertz (Hz). The following abbreviations are used for the multiplicity of NMR signals: s, singlet; d, doublet; t, triplet; q, quartet; dd, doublet of doublets; br.s, broadened signal; m, multiplet. The elemental analysis was performed utilizing a Perkin Elmer 2400 CHN analyzer. Melting points were determined on a Stuart SMP3 (Staffordshire, UK) and are uncorrected.

UV/Vis absorption spectra were recorded on Shimadzu UV1800 spectrophotometer, fluorescence emission spectra, absolute quantum yields and lifetimes of luminescence were recorded on Edinburgh FS5 and Horiba FluoroMax spectrofluorometers integrated with integration sphere and TCSPC with a nanosecond LED (370 nm), respectively. Solvatochromic studies were carried out using a Solar CM2203 spectrofluorimeter.

Quantum-chemical calculations were performed using the ORCA 6.0 program package [49]. Geometry optimizations and thermodynamic parameter calculations were carried out within the framework of density functional theory at the  $\omega\text{B97X-D4/ma-def2-TZVP}$  level of theory. The D4 dispersion correction was applied to account for long-range and noncovalent interactions [50–52]. The RJCOSX approximation in combination with auxiliary def2/J basis sets was employed to accelerate the calculations. Tight convergence criteria for the self-consistent field procedure were ensured using the TIGHTSCF keyword. Frequency calculations were performed for all optimized structures, and the absence of imaginary frequencies confirmed that the optimized geometries correspond to true local minima on the potential energy surface.

Solvation effects in dimethyl sulfoxide (DMSO) were modeled using the SMD continuum solvation model as implemented in ORCA. Solvation energy calculations were performed using compound **4a** as a representative system.

When evaluating thermodynamic parameters, the formation of anionic species upon solvation, as well as the formation of sodium–DMSO ion pairs, was taken into account [53].

Electronic excited states were calculated using time-dependent density functional theory (TD-DFT) at the B3LYP/def2-TZVP level of theory [54]. The lowest five singlet excited states were computed, and excitation energies and oscillator strengths were obtained.

Wavefunction analyses, including molecular orbital composition and electronic transition characteristics, were performed using the Multiwfn program [55]. Visualization of molecular orbitals and electronic transitions was carried out with GaussView 6.0 [56].

Compounds **2a** and **2d** were synthesized according to the previously reported procedure [36].

Compounds **2b**, **2g** were synthesized according to the procedure: The suspension of appropriate 7-(4-(dimethylamino)phenyl)-6-hydroxy-[1,2,4]azolo[1,5-a]pyrimidine-5-carbonitrile (1 mmol) and sodium hydroxide (1 mmol) in a mixture of water (5 mL) and ethanol (5 mL) was sonicated for 20 min, after which the reaction mass was heated on an oil bath until it was completely dissolved. Then, the solution was evaporated under reduced pressure, the residue was crystallized from isopropyl alcohol, and the precipitate was filtered out.

**Sodium 5-cyano-7-(4-(dimethylamino)phenyl)-2-methyl-[1,2,4]triazolo[1,5-a]pyrimidin-6-olate pentahydrate (2b)**. Red powder (95%), m.p.: 215–217 °C (decompose).  $^1\text{H}$  NMR (400 MHz, DMF-D7)  $\delta$  8.70 (d,  $J = 9.2$  Hz, 2H), 6.78 (d,  $J = 9.3$  Hz, 2H), 3.03 (s, 6H), 2.37 (s, 3H).  $^{13}\text{C}$  NMR (101 MHz, DMF-D7)  $\delta$  158.9, 151.4, 148.8, 134.0, 132.5, 131.0, 130.6, 120.6, 119.6, 111.2, 40.5, 15.5. Calcd for  $\text{C}_{15}\text{H}_{13}\text{N}_6\text{NaO}\cdot 5\text{H}_2\text{O}$ : C, 44.33; H, 5.71; N, 20.68, found C, 44.42; H, 5.76; N, 20.56.

**Sodium 5-cyano-7-(4-(dimethylamino)phenyl)-3-(ethoxycarbonyl)pyrazolo[1,5-a]pyrimidin-6-olate dihydrate (2g)**. Red powder (82%), m.p.: 275–277 °C (decompose).  $^1\text{H}$  NMR (400 MHz, DMF-D7)  $\delta$  8.47 (d,  $J = 9.0$  Hz, 2H), 8.24 (s, 1H), 6.77 (d,  $J = 9.2$  Hz, 2H), 4.27 (q,  $J = 7.1$  Hz, 2H), 1.32 (t,  $J = 7.1$  Hz, 3H).  $^{13}\text{C}$  NMR (101 MHz, DMF-D7)  $\delta$  158.7, 151.4, 146.7, 139.7, 134.6, 132.9, 132.1, 120.4, 119.1, 111.1, 100.2, 59.7, 40.5, 15.3. Calcd for  $\text{C}_{18}\text{H}_{16}\text{N}_5\text{NaO}_3\cdot 2\text{H}_2\text{O}$ : C, 52.81; H, 4.92; N, 17.11, found C, 51.35; H, 5.29; N, 18.01

**General procedure for the synthesis of compounds 2c, 2e, 2f, 2h** The suspension of appropriate 7-(4-(dimethylamino)phenyl)-6-hydroxy-[1,2,4]azolo[1,5-a]pyrimidine-5-carbonitrile (1 mmol) and sodium hydroxide (1 mmol) in a mixture of water (5 mL) and ethanol (5 mL) was sonicated for 1 min, after which the reaction mass was heated on an oil bath until it was completely dissolved. Then, the solution was cooled to room temperature, and the precipitate was filtered out and washed with small amount of water.

**Sodium 5-cyano-7-(4-(dimethylamino)phenyl)-2-phenyl-[1,2,4]triazolo[1,5-a]pyrimidin-6-olate pentahydrate (2c).** Red powder (92%), m.p.: 169–171 °C (decompose). <sup>1</sup>H NMR (400 MHz, DMF- D7) δ 8.81 (d, J = 8.6 Hz, 2H), 8.23 (m, 2H), 7.48 (m, 3H), 6.82 (d, J = 8.7 Hz, 2H), 3.06 (s, 6H). <sup>13</sup>C NMR (101 MHz, DMF- D7) δ 151.5, 149.2, 134.3, 133.5, 132.6, 131.8, 130.5, 129.6, 127.6, 120.5, 119.3, 111.2, 40.5. Calcd for C<sub>20</sub>H<sub>15</sub>N<sub>6</sub>NaO·5H<sub>2</sub>O: C, 51.28; H, 5.38; N, 17.94, found C, 51.42; H, 5.22; N, 17.90.

**Sodium 5-cyano-7-(4-(dimethylamino)phenyl)-2-(thiophen-2-yl)-[1,2,4]triazolo[1,5-a]pyrimidin-6-olate tetrahydrate (2e).** Red powder (83%), m.p.: 180–182 °C (decompose). <sup>1</sup>H NMR (400 MHz, DMF-D7) δ 8.78 (d, J = 9.2 Hz, 2H), 7.76 (dd, J = 3.6, 1.2 Hz, 1H), 7.66 (dd, J = 5.0, 1.2 Hz, 1H), 7.20 (dd, J = 5.0, 3.6 Hz, 1H), 6.82 (d, J = 9.2 Hz, 2H), 3.06 (s, 6H). <sup>13</sup>C NMR (101 MHz, DMF-D7) δ 160.6, 159.5, 151.5, 148.5, 136.7, 134.2, 132.6, 131.5, 128.9, 128.4, 127.3, 120.6, 119.5, 111.2, 40.5. Calcd for C<sub>18</sub>H<sub>13</sub>N<sub>6</sub>NaOS·4H<sub>2</sub>O: C, 47.36; H, 4.64; N, 18.41, found C, 47.44; H, 4.46; N, 18.52.

**Sodium 5-cyano-7-(4-(dimethylamino)phenyl)-2-(furan-2-yl)-[1,2,4]triazolo[1,5-a]pyrimidin-6-olate tetrahydrate (2f).** Red powder (87%), m.p.: 123–125 °C (decompose). <sup>1</sup>H NMR (400 MHz, DMF-D7) δ 8.90 (d, J = 9.2 Hz, 2H), 8.21 (s, 1H), 7.26 (d, J = 3.4 Hz, 1H), 6.99 (d, J = 9.2 Hz, 2H), 6.85 (dd, J = 3.4, 1.8 Hz, 1H), 3.23 (s, 6H). <sup>13</sup>C NMR (101 MHz, DMF-D7) δ 159.3, 157.7, 151.5, 148.9, 148.4, 145.0, 134.3, 132.6, 131.7, 120.5, 119.4, 112.8, 111.2, 110.9, 40.5. Calcd for C<sub>18</sub>H<sub>13</sub>N<sub>6</sub>NaO<sub>2</sub>·4H<sub>2</sub>O: C, 49.09; H, 4.81; N, 19.08, found C, 49.19; H, 4.98; N, 19.19

**Sodium 3,5-dicyano-7-(4-(dimethylamino)phenyl)-2-(methylthio)pyrazolo[1,5-a]pyrimidin-6-olate tetrahydrate (2h).** Red powder (85%), m.p.: 209–211 °C (decompose). <sup>1</sup>H NMR (400 MHz, DMF-D7) δ 7.91 (d, J = 9.1 Hz, 2H), 6.47 (d, J = 8.5 Hz, 2H), 3.08 (s, 6H), 2.68 (s, 3H). <sup>13</sup>C NMR (101 MHz, DMF-D7) δ 158.7, 152.1, 148.4, 146.6, 138.5, 133.2, 131.0, 117.6, 114.3, 113.8, 110.4, 79.3, 40.1, 14.1. Calcd for C<sub>17</sub>H<sub>13</sub>N<sub>6</sub>NaOS·4H<sub>2</sub>O: C, 45.94; H, 4.76; N, 18.91, found C, 46.04; H, 4.64; N, 18.95.

### Supplementary materials

This manuscript contains supplementary materials, which are available on the corresponding online page.

### Data availability statement

The data supporting the findings of this study are available from the corresponding author upon reasonable request.

### Acknowledgments

To the memory of our teacher and mentor, Professor E.N. Ulomsky (01.10.1961–04.08.2025).

### Author contributions

Conceptualization: A.S.V., F.V.V., K.D.S., R.V.L.  
Data curation: K.E.A., A.S.V., F.V.V., K.D.S.  
Formal Analysis: K.E.A., T.A.N., A.S.V., M.T.D.  
Investigation: K.E.A., A.S.V., T.A.N., S.Y.M.  
Project administration: F.V.V.

Resources: V.M.V.

Software: T.A.N.

Supervision: R.V.L., Z.G.V., V.M.V.

Visualization: K.E.A., T.A.N.

Writing – original draft: A.S.V., F.V.V., T.A.N.

Writing – review & editing: F.V.V., M.T.D., V.M.V., R.V.L., Z.G.V.

### Conflict of interest

The authors declare no conflict of interest

### Additional information

Author IDs:

Semen V. Aminov, Scopus ID [57981648100](https://orcid.org/0009-0001-57981648100);  
Victor V. Fedotov, Scopus ID: [56320225200](https://orcid.org/0009-0002-56320225200);  
Dmitry S. Kopchuk, Scopus ID [14123383900](https://orcid.org/0009-0001-14123383900);  
Ekaterina A. Kudryashova, Scopus ID [57359251800](https://orcid.org/0009-0001-57359251800);  
Yulia M. Sayfutdinova, Scopus ID [59308210300](https://orcid.org/0009-0001-59308210300);  
Timofey D. Moseev, Scopus ID [57196048249](https://orcid.org/0009-0001-57196048249);  
Mikhail V. Varaksin, Scopus ID [26637829900](https://orcid.org/0009-0001-26637829900);  
Anton N. Tsmokalyuk, Scopus ID [56784365100](https://orcid.org/0009-0001-56784365100);  
Grigoriy V. Zyryanov, Scopus ID [6701496404](https://orcid.org/0009-0001-6701496404);  
Vladimir L. Rusinov, Scopus ID [7006493788](https://orcid.org/0009-0001-7006493788).

Websites:

Ural Federal University named after the First President of Russia B.

N. Yeltsin: <https://urfu.ru/ru>

Postovsky Institute of Organic Synthesis: <https://iosuran.ru>

### References

- Ghosh S, Rana A, Biswas S. Metal–Organic Framework-Based Fluorescent Sensors for the Detection of Pharmaceutically Active Compounds. *Chem. Mater.* 2024;36(1):99–131. doi:10.1021/acs.chemmater.3c02459
- Liu H, Jiang G, Ke G, Ren T-B, Yuan L. Organic fluorophores with large Stokes shift for bioimaging and biosensing. *Chem-PhotoChem.* 2024;8(5):e202300277. doi:10.1002/cptc.202300277
- Gagarin AA, Minin AS, Shevyrin VA, Benassi E, Belskaya NP. Photocaging of amino acids and short peptides by aryli-denethiazoles: mechanism, photochemical characteristics and biological behaviour. *J. Mater. Chem. B.* 2024;12(44):11402–11413. doi:10.1039/D4TB01441C
- Elkina NA, Shchegolkov EV, Burgart YV, Steparuk AS, Gazizov DA, Osminin AE, Zhilina EF, Minin AS, Gerasimova NA, Evstigneeva NP, Saloutin VI. 5-(Trifluoromethyl)-4-biarylhy-drazinylidenepyrazol-3-ones: synthesis, photophysical and biological properties. *Dyes Pigm.* 2026;246:113264. doi:10.1016/j.dyepig.2025.113264
- Steparuk AS, Irgashev RA, Zhilina EF, Rusinov GL, Petrova SA, Saranin DS, Aleksandrov AE, Tameev AR, Thieno[3,2-b]indole-benzo[b]thieno[2,3-d]thiophen-3(2H)-one-based D-π-A molecules as electron transport materials for perovskite solar cells. *New J. Chem.* 2022;46:16612–16617. doi:10.1039/D2NJ02202H
- Diguet C, Navarro A, Fernández-Lienres MP, Jiménez-Pulido SB, Illán-Cabeza NA, Almutairi A, Tondelier D, Gauthier S, Robin-le Guen F, Rodríguez-López J, Massue J, Achelle S. Pyrimidine-based four-coordinate O<sup>N</sup>^O boron complexes: synthesis, photophysical and theoretical studies, and TADF-based OLED devices. *Chem. - Eur. J.* 2025;e202501089. doi:10.1002/chem.202501089
- Amna B, Isci R, Siddiqi HM, Majewski LA, Faraji S, Ozturk T. Organic field-effect transistor-based sensors: recent progress, challenges and future outlook. *J. Mater. Chem. C* 2025;13(17):8354–8424. doi:10.1039/D4TC04265D
- Pinheiro S, Pinheiro EMC, Muri EMF, Pessôa JC, Cadorini MA, Greco SJ. Biological activities of [1,2,4]triazolo[1,5-a]pyrimidines and analogs. *Med. Chem. Res.* 2020;29:1751–1776. doi:10.1007/s00044-020-02609-1

9. Hammouda MM, Gaffer HE, Elattar KM. Insights into the medicinal chemistry of heterocycles integrated with a pyrazolo[1,5-a]pyrimidine scaffold. *RSC Med. Chem.* 2022;13:1150–1196. doi:10.1039/D2MD00192F
10. Tigreros A, Aranzazu SL, Bravo NF, Zapata-Rivera J, Portilla J. Pyrazolo[1,5-a]pyrimidines-based fluorophores: a comprehensive theoretical-experimental study. *RSC Adv.* 2020;10:39542–39552. doi:10.1039/DoRA07716J
11. Bouihi F, Schmaltz B, Mathevet F, Kreher D, Faure-Vincent J, Yildirim C, Elhakmaoui A, Bouclé J, Akssira M, Tran-Van F, Abarbi M. D- $\pi$ -A-Type pyrazolo[1,5-a]pyrimidine-based hole-transporting materials for perovskite solar cells: effect of the functionalization position. *Materials.* 2022;15(22):7992. doi:10.3390/ma15227992
12. Rapolu R, Bhusanur DI, Puyad AL, Bhosale SV, et al. Aggregation induced emission based on benzo[4,5]thiazolo[3,2-a]pyrimidine-3-carbonitrile fused tetraphenylethylene for visualization of latent fingerprints and anticounterfeiting applications. *J. Mol. Struct.* 2025;1334:141937. doi:10.1016/j.mol-struct.2025.141937
13. Yang XZ, Sun R, Guo X, Wei XR, Gao J, Xu YJ, Ge JF. The application of bioactive pyrazolopyrimidine unit for the construction of fluorescent biomarkers. *Dyes Pigm.* 2020;173:107878. doi:10.1016/j.dyepig.2019.107878
14. Ye DY, Dong ZY, Pu YQ, Huang GW, An Y, Lü CW. Design of two large conjugate triazolopyrimidine analogs and their application in detection of 2,4,6-trinitrophenol. *Dyes Pigm.* 2020;174:108016. doi:10.1016/j.dyepig.2019.108016
15. Ju KS, Parales RE. Nitroaromatic compounds, from synthesis to biodegradation. *Microbiol. Mol. Biol. Rev.* 2010;74(2):250–272. doi:10.1128/MMBR.00006-10
16. Millar RW, Philbin SP, Claridge RP, Hamid J. Selection and synthesis of energetic heterocyclic compounds: rationale and examples. *Propellants, Explos., Pyrotech.* 2008;33(1):66–72. doi:10.1002/prep.200800211
17. Meyer R, Köhler J, Homburg A. Explosives. Wiley-VCH Verlag GmbH & Co. KGaA: Weinheim, Germany; 2016. 1036 p.
18. Conkling JA, Mocella C. *Chemistry of Pyrotechnics: Basic Principles and Theory.* CRC Press: Boca Raton, FL, USA; 2019. 460 p.
19. Bilal M, Bagheri AR, Bhatt P, Chen S. Environmental occurrence, toxicity concerns, and remediation of recalcitrant nitroaromatic compounds. *J. Environ. Manage.* 2021;291:112685. doi:10.1016/j.jenvman.2021.112685
20. Gruzov VM, Baldin MN, Makas' AL, Titov BG. Progress in methods for the identification of explosives in Russia. *J. Anal. Chem.* 2011;66(11):1121–1131. doi:10.1134/S1061934811110074
21. Brown KE, Greenfield MT, McGrane SD, Moore DS. Advances in explosives analysis – Part I: animal, chemical, ion, and mechanical methods. *Anal. Bioanal. Chem.* 2016;408(1):35–47. doi:10.1007/s00216-015-9040-4
22. Brown KE, Greenfield MT, McGrane SD, Moore DS. Advances in explosives analysis – Part II: photon and neutron methods. *Anal. Bioanal. Chem.* 2016;408(1):49–65. doi:10.1007/s00216-015-9043-1
23. Goldman ER, Anderson GP, Lebedev N, Lingerfelt BM, Winter PT, Patterson CH Jr, Mauro JM. Analysis of aqueous 2,4,6-trinitrotoluene (TNT) using a fluorescent displacement immunoassay. *Anal. Bioanal. Chem.* 2003;375(4):471–475. doi:10.1007/s00216-002-1713-0
24. Steinfeldt JI, Wormhoudt J. Explosives detection: a challenge for physical chemistry. *Annu Rev. Phys. Chem.* 1998;49:203–232. doi:10.1146/annurev.physchem.49.1.203
25. Moore DS. Instrumentation for trace detection of high explosives. *Rev. Sci. Instrum.* 2004;75(8):2499–2512. doi:10.1063/1.1771493
26. Singh S. Sensors—an effective approach for the detection of explosives. *J. Hazard. Mater.* 2007;144(1-2):15–28. doi:10.1016/j.jhazmat.2007.02.018
27. Jiménez AM, Navas MJ. Chemiluminescence detection systems for the analysis of explosives. *J. Hazard. Mater.* 2004;106(1):1–5. doi:10.1016/j.jhazmat.2003.07.005
28. Agrawal JP. High Energy Materials: Propellants, Explosives and Pyrotechnics. Hoboken, NJ: John Wiley & Sons; 2010. 466 p.
29. Peng Y, Zhang AJ, Dong M, Wang YW. A colorimetric and fluorescent chemosensor for the detection of an explosive—2,4,6-trinitrophenol (TNP). *Chem. Commun.* 2011;47:4505–4507. doi:10.1039/C1CC10400D
30. Hu Z, Deibert BJ, Li J. Luminescent metal-organic frameworks for chemical sensing and explosive detection. *Chem. Soc. Rev.* 2014;43:5815–5840. doi:10.1039/C4CS00010B
31. O'Mahony AM, Wang J. Nanomaterial-based electrochemical detection of explosives: a review of recent developments. *Anal. Methods.* 2013;5(17):4296–4309. doi:10.1039/C3AY40636A
32. Zhao Z, Liu J, Lam JWY, Chan CYK, Qiu H, Tang BZ. Luminescent aggregates of a starburst silole-triphenylamine adduct for sensitive explosive detection. *Dyes Pigm.* 2011;91(2):258–263. doi:10.1016/j.dyepig.2011.03.006
33. Patil PDJ, Wagalgave SM, Ingle RD, Nanubolu JB, Bhosale RS, Bhosale SV, Pawar RP. Merocyanine-benzothiazole chromophore-based sensor for selective picric acid detection. *ChemistrySelect.* 2019;4(34):10013–10020. doi:10.1002/slct.201902722
34. Sivaraman G, Vidya B, Chellappa D. Rhodamine based selective turn-on sensing of picric acid. *RSC Adv.* 2014;4(58):30828–30831. doi:10.1039/C4RA02931C
35. Verbitskiy EV, Baranova AA, Lugovik KI, Khokhlov KO, Cheprakova EM, Rusinov GL, Chupakhin ON, Charushin VN. New 2-H-[1,2,3]triazolo[4,5-e][1,2,4]triazolo[1,5-a]pyrimidine derivatives as D- $\pi$ -A dyes. *Tetrahedron.* 2016;72:4954–4961. doi:10.1016/j.tet.2016.06.071
36. Aminov SV, Fedotov VV, Moseev TD. Hydroperoxide-induced nitrile migration in azolo[1,5-a]pyrimidine-6-carbonitriles: an original approach toward functionalized azolopyrimidines. *J. Org. Chem.* 2025;90(37):12888–12903. doi:10.1021/acs.joc.5c00896
37. Kosower EM. The effect of solvent on spectra. I. A new empirical measure of solvent polarity: Z-values. *J. Am. Chem. Soc.* 1958;80:3253–3260. doi:10.1021/jao1546a020
38. Dimroth K, Reichardt C, Siepmann T, Bohlmann F. Über Pyridinium-N-phenol-betaine und ihre Verwendung zur Charakterisierung der Polarität von Lösungsmitteln. *Justus Liebigs Ann. Chem.* 1963;661:1–37. doi:10.1002/jlac.19636610102
39. Skoog DA, Holler FJ, Crouch SR, editors. *Encyclopedia of Analytical Chemistry: Applications, Theory and Instrumentation.* John Wiley & Sons: Chichester, UK; 2000. 14 752 p. doi:10.1007/978-0-387-46312-4
40. Kvashnin YA, Zhilina EF, Gazizov DA, Mekhaev AV, et al. Conversion of tetraphenylethylene-substituted oxadiazolo[3,4-b]pyrazines into the corresponding imidazo[4,5-b]- and pyrazino[2,3-b]pyrazines, as chemosensors for the selective detection of nitroaromatics in aqueous media. *Dyes Pigm.* 2024;228:112253. doi:10.1016/j.dyepig.2024.112253
41. Li Y, Liu K, Li W-J, Guo A, Zhao F-Y, Liu H, Ruan W-J. Coordination Polymer Nanoarchitecture for Nitroaromatic Sensing by Static Quenching Mechanism. *J. Phys. Chem.* 2015;119:28544–28550. doi: 10.1021/acs.jpcc.5b08259
42. Shrivastava A, Gupta VB. Methods for the determination of limit of detection and limit of quantitation of the analytical methods. *Chron. Young. Sci.* 2011;2(1):21–25. doi:10.4103/2229-5186.79345
43. Sadieva LK, Khasanov AF, Shendrikova TI, Nikonov IL, Koptchuk DS, Taniya OS, Kim GA, Novikov AS, Shabunina OV, Zyryanov GV, Charushin VN. (Het)aryl-substituted mono-azatriphenylenes as luminescent “turn-off” chemosensors for nitroaromatic compounds with internal filter effect correction. *Opt. Mater.* 2025;162:116949. doi:10.1016/j.optmat.2025.116949

44. Chen B, Chai S, Liu J, Liu C, Li Y, He J, Yu Z, Yang T, Feng C, Huang C. 2,4,6-Trinitrophenol detection by a new portable sensing gadget using carbon dots as a fluorescent probe. *Anal. Bioanal. Chem.* 2019;411(11):2291–2300. [doi:10.1007/s00216-019-01670-z](https://doi.org/10.1007/s00216-019-01670-z)
45. Kathiravan A, Gowri A, Khamrang T, Deepan Kumar M, Dhenadhayalan N, Lin KC, Velusamy M, Jaccob M. Pyrene-Based Chemosensor for Picric Acid – Fundamentals to Smartphone Device Design. *Anal. Chem.* 2019;91(20):13244–13250. [doi:10.1021/acs.analchem.9b03695](https://doi.org/10.1021/acs.analchem.9b03695)
46. Zhang E, Ju P, Guo P, Hou X, Hou X, Lv H, Wang J, Zhang Y. A FRET-based fluorescent and colorimetric probe for the specific detection of picric acid. *RSC Adv.* 2018;8:31658–31665. [doi:10.1039/c8ra05468a](https://doi.org/10.1039/c8ra05468a)
47. Lin C, He X, Xi C, Zhang Q, Wang LW. Ion solvation free energy calculations based on first-principles molecular dynamics thermodynamic integration. *J. Chem. Phys.* 2024;160(18):184115. [doi:10.1063/5.0191068](https://doi.org/10.1063/5.0191068)
48. Jacquemin D, Perpète EA, Scalmani G, Frisch MJ, Kobayashi R, Adamo C. Time-dependent density functional theory for electronic excited states: assessment of accuracy. *J. Chem. Theory Comput.* 2008;4:123–135. [doi:10.1021/ct700187k](https://doi.org/10.1021/ct700187k)
49. Neese F. The ORCA program system. *WIREs Comput. Mol Sci.* 2018;8:e1327. [doi:10.1002/wcms.1327](https://doi.org/10.1002/wcms.1327)
50. Chai JD, Head-Gordon M. Long-range corrected hybrid density functionals with damped atom–atom dispersion corrections. *Phys. Chem. Chem. Phys.* 2008;10:6615–6620. [doi:10.1039/B810189B](https://doi.org/10.1039/B810189B)
51. Caldeweyher E, Ehlert S, Hansen A, Neugebauer H, Spicher S, Bannwarth C, Grimme S. A generally applicable atomic-charge dependent London dispersion correction. *J. Chem. Phys.* 2019;150:154122. [doi:10.1063/1.5090222](https://doi.org/10.1063/1.5090222)
52. Weigend F, Ahlrichs R. Balanced basis sets of split valence, triple zeta valence and quadruple zeta valence quality for H to Rn. *Phys. Chem. Chem. Phys.* 2005;7:3297–3305. [doi:10.1039/B508541A](https://doi.org/10.1039/B508541A)
53. Marenich AV, Cramer CJ, Truhlar DG. Universal solvation model based on solute electron density and a continuum model of the solvent. *J. Phys. Chem. B.* 2009;113:6378–6396. [doi:10.1021/jp810292n](https://doi.org/10.1021/jp810292n)
54. Casida ME. Time-dependent density functional response theory for molecules. In: Chong DP, editor. *Recent Advances in Density Functional Methods. Part I.* Singapore: World Scientific; 1995. p. 155–192. [doi:10.1142/9789812830586\\_0005](https://doi.org/10.1142/9789812830586_0005)
55. Lu T, Chen F. Multiwfn: a multifunctional wavefunction analyzer. *J. Comput. Chem.* 2012;33:580–592. [doi:10.1002/jcc.22885](https://doi.org/10.1002/jcc.22885)
56. Dennington R, Keith T, Millam J. GaussView. Version 6.0. Shawnee Mission, KS: Semichem Inc.; 2016. Available from: <https://gaussian.com/gaussview6/>